Letter

Magnon corner states in twisted bilayer honeycomb magnets

Chun-Bo Hua,[1,2,*] Feiping Xiao,[3,*] Zheng-Rong Liu,[4,*] Jin-Hua Sun,[5] Jin-Hua Gao,[6] Chui-Zhen Chen,[7] Qingjun Tong,[3,†] Bin Zhou,[4,‡] and Dong-Hui Xu[8,9,§]

[1]*School of Electronic and Information Engineering, Hubei University of Science and Technology, Xianning 437100, China*
[2]*Laboratory of Optoelectronic Information and Intelligent Control, Hubei University of Science and Technology, Xianning 437100, China*
[3]*School of Physics and Electronics, Hunan University, Changsha 410082, China*
[4]*Department of Physics, Hubei University, Wuhan 430062, China*
[5]*Department of Physics, Ningbo University, Ningbo 315211, China*
[6]*School of Physics and Wuhan National High Magnetic Field Center, Huazhong University of Science and Technology, Wuhan 430074, China*
[7]*Institute for Advanced Study and School of Physical Science and Technology, Soochow University, Suzhou 215006, China*
[8]*Department of Physics and Chongqing Key Laboratory for Strongly Coupled Physics, Chongqing University, Chongqing 400044, People's Republic of China*
[9]*Center of Quantum Materials and Devices, Chongqing University, Chongqing 400044, People's Republic of China*

(Received 22 June 2022; revised 2 December 2022; accepted 3 January 2023; published 12 January 2023)

The study of symmetry-protected topological phases of matter has been extended from fermionic electron systems to various bosonic systems. Bosonic topological magnon phases in magnetic materials have received much attention because of their exotic uncharged topologically protected boundary modes and the potential for dissipationless magnonics and spintronic applications. Here, we establish twisted bilayer honeycomb magnets as a platform for hosting second-order topological magnon insulators (SOTMIs) without fine-tuning. We employ a simple, minimal Heisenberg spin model to describe misaligned bilayer sheets of honeycomb ferromagnetic magnets with a large commensurate twist angle. We found that the higher-order topology in this bilayer system shows a significant dependence on the interlayer exchange coupling. The SOTMI, featuring topologically protected magnon corner states that go beyond the conventional bulk-boundary correspondence, appears for ferromagnetic interlayer couplings, while the twisted bilayer exhibits a nodal phase in the case of antiferromagnetic interlayer coupling. At last, relevance to twisted bilayer CrI_3 is also discussed.

DOI: 10.1103/PhysRevB.107.L020404

Introduction. After the discovery of time-reversal invariant topological insulators, symmetry-protected topological phases of matter have been an exciting and cutting-edge area of research in condensed matter physics [1–6]. Remarkably, symmetry-protected topological phases are not unique to electronic systems, and have been identified in various bosonic systems either, where topological magnon phases have received special attention for their potential applications in spintronics [7–10]. Up to now, fruitful topological magnon phases including insulating and semimetallic phases, have been investigated both theoretically and experimentally [11–59]. Recently, the concept of higher-order topological insulators [60–64] has been extended to magnonic systems as well [65–70]. The hallmark feature of an nth-order magnon topological insulator in d dimensions is the existence of protected gapless magnon states at its $(d-n)$-dimensional boundaries, which go beyond the celebrated bulk-boundary correspondence. For example, a second-order topological magnon insulator (SOTMI) with magnon corner states is realized in a ferromagnetic (FM) Heisenberg model on a two-dimensional (2D) breathing kagome lattice [65], a magnonic quadrupole topological insulator hosting magnon corner states can appear in 2D antiskyrmion crystals [66], and a SOTMI with 1D chiral hinge magnons is predicted to be realized in 3D stacked honeycomb magnets [67]. All these existing magnonic higher-order topological insulators require significant Dzyaloshinskii-Moriya interaction, whereas the Dzyaloshinskii-Moriya interaction is a typically weak effect in most magnetic materials [71,72].

In recent years, 2D twisted van der Waals materials have emerged as a versatile platform for studying exotic and elusive states of matter, following the discovery of unconventional superconductivity [73] and the Mott insulator [74] in twisted bilayer graphene (TBG) with magic angles [75]. TBG has been shown to yield a series of fascinating correlated and topological phenomena [75–85]. Besides the intrinsic fragile topology [86–89] of the nearly flat bands, higher-order band topology has been subsequently identified in TBG as well [90–93]. Meanwhile, researchers have turned their attention to twisted bilayer honeycomb magnets (TBHMs) analogous to twisted bilayer graphene, and revealed rich magnetic phases caused by moiré patterns as well as intriguing moiré magnetic excitations in TBHMs [94–97]. Moreover, moiré magnetism has been reported in twisted bilayer CrI_3 [98–100] in a very

*These authors contributed equally to this work.
†tongqj@hnu.edu.cn
‡binzhou@hubu.edu.cn
§donghuixu@cqu.edu.cn

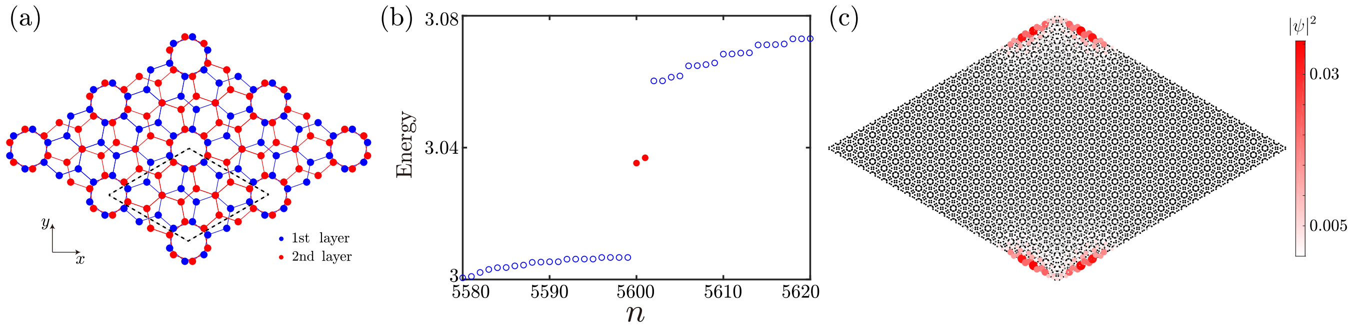

FIG. 1. (a) Schematic illustration of the TBHM lattice with the large commensurate angle $\theta = 21.78^{\circ}$. Blue dots represent the first layer lattice and red dots represent the second layer lattice. The blue (red) lines denote the first (second) layer intralayer nearest-neighbor bonds. The rhombus shaped area composed of the black thick dashed lines represents a single moiré unit cell. (b) Magnon energy spectrum of the Hamiltonian [Eq. (3)] of the rhombus-shaped TBHM system versus the eigenvalue index n. Red dots mark the in-gap magnon corner states. (c) The spatial distribution of the probability density of the two in-gap states in (b). The color map shows the values of the probability density. We take the exchange coupling ratio $J_{\perp}/J = 0.2$, and the lattice site number $N = 11200$.

recent experiment. Inspired by the recent theoretical and experimental developments in twisted 2D magnets, it is tempting to ask whether higher-order topological magnon insulators can occur in TBHMs.

In this work, we reveal that a SOTMI can be realized in the TBHM at the large commensurate angle, without requiring the Dzyaloshinskii-Moriya interaction. We adopt a simple, minimal spin model which consists of two honeycomb FM layers with the nearest-neighbor intralayer exchange interaction coupled by the FM or antiferromagnetic (AFM) interlayer exchange coupling, to describe the TBHMs with collinear order. For our purpose, we assume that the interlayer exchange coupling is sufficiently weak compared to the intralayer Heisenberg interaction. Therefore, the out-of-plane collinear magnetic order is favored under weak interlayer coupling. Furthermore, we obtain an effective magnon Hamiltonian in terms of the Holstein-Primakoff transformation to bosonize the spin model. Based on numerical diagonalization, we show that the FM interlayer coupling can give rise to an energy gap associated with the nontrivial higher-order topology characterized by a mirror winding number, resulting in a SOTMI in the TBHM. The SOTMI supports two in-gap magnon corner states localized at mirror symmetric corners. The magnon corner states are robust against symmetry-preserving disorder. In contrast, in the case of AFM interlayer coupling, the TBHM system remains gapless and has magnon Dirac dispersion. Our work, together with these works on higher-order topology in twisted photonic [101,102] and acoustic [103] materials, suggest a natural strategy to realize bosonic higher-order topological insulators.

Model. We consider a twisted AA-stacked bilayer honeycomb magnets with the commensurate angle $\theta = 21.78^{\circ}$, whose spins are localized at the hexagon vertices marked by red and blue dots, as shown in Fig. 1(a). The spin Hamiltonian is formulated on the twisted bilayer honeycomb lattice, which reads

$$H = -J \sum_{\langle i,j\rangle,l} \mathbf{S}_{i,l} \cdot \mathbf{S}_{j,l} - J_{\perp} \sum_{\langle i,j\rangle} \mathbf{S}_{i,2} \cdot \mathbf{S}_{j,1}, \tag{1}$$

where the first and second terms represent the nearest-neighbor intralayer and nearest-neighbor interlayer Heisenberg interactions, respectively. $\mathbf{S}_{i,l} = (S^x_{i,l}, S^y_{i,l}, S^z_{i,l})$ is the spin vector operator at site i on layer $l = 1, 2$, and the summation runs over nearest-neighbor sites $\langle i, j\rangle$. $J > 0$ denotes the FM intralayer interaction, and $J_{\perp}$ is a tunable parameter in TBHMs, which is positive for the FM interlayer coupling while negative for the AFM coupling. Here, $J_{\perp}$ only couples the sites of the first layer with the sites of the second layer that are positioned directly next to them. In the Supplemental Material (SM) [104], we also show the results when including the spatially modulated remote interlayer couplings.

Noticing that the twisted bilayer system is constructed by twisting the bilayer magnets with respect to the collinear axis at the hexagonal center, where the lower layer rotates counterclockwise $\theta/2$ and the upper layer rotates clockwise $\theta/2$, respectively. The system belongs to D_6 point group [90] with concurrent spatial and spin rotations. More specifically, the system is invariant under the action of either of the symmetry operators: C_{6z}, sixfold rotation about the out-of-plane z axis, and $C_{2x/2y}$, twofold rotation about the in-plane x/y axis.

In the FM case, the classical ground state is represented by the uniform state $\mathbf{S}_{i,l} \equiv S\hat{\mathbf{z}}$, where the spins point along the $+z$ direction. In the ordered phase supported at sufficiently low temperatures, we obtain an effective magnon Hamiltonian through the linear spin-wave theory. Using the Holstein-Primakoff transformation [105]

$$\begin{aligned} S_i^+ &= S_i^x + iS_i^y \simeq \sqrt{2S}d_i, \\ S_i^- &= S_i^x - iS_i^y \simeq \sqrt{2S}d_i^{\dagger}, \\ S_i^z &= S - d_i^{\dagger}d_i, \end{aligned} \tag{2}$$

and neglecting magnon-magnon interactions, the spin Hamiltonian can be transformed into a quadratic magnon Hamiltonian

$$\begin{aligned} H =& 3JS\sum_{i,l} d_{i,l}^{\dagger}d_{i,l} - JS\sum_{\langle i,j\rangle,l}(d_{i,l}^{\dagger}d_{j,l} + \text{H.c.}) \\ &+ J_{\perp}S\sum_{\langle i,j\rangle}[(d_{i,2}^{\dagger}d_{i,2} + d_{j,1}^{\dagger}d_{j,1}) - (d_{i,2}^{\dagger}d_{j,1} + \text{H.c.})], \end{aligned} \tag{3}$$

where $d_i^{\dagger}$ (d_i) is the bosonic creation (annihilation) operator. In subsequent calculations, the energy unit is set as the intralayer Heisenberg interaction amplitude J. In addition, the lattice

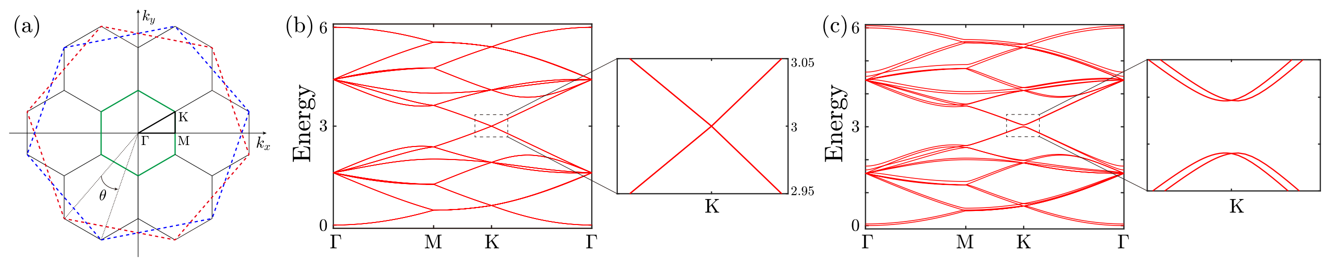

FIG. 2. (a) Moiré Brillouin zone. The dashed red (first layer) and blue (second layer) large hexagons show the unfolded Brillouin zones of individual layers, respectively, and the blue hexagon corresponds to red hexagon for the twist angle $\theta = 21.78^\circ$. The first moiré Brillouin zone of the bilayer is shown by the central (green) thick solid hexagon. The next several Brillouin zones of the TNHM are depicted by the six surrounding (black) thin solid hexagons. The magnon band structures are calculated along the high symmetry path specified by the triangle ΓMK (black). The symmetry points are $\Gamma = (0, 0)$, $\mathrm{M} = (2\sqrt{7}\pi/21, 0)$, and $\mathrm{K} = (2\sqrt{7}\pi/21, 2\sqrt{21}\pi/63)$. (b) Magnon band structure of the TBHM with $\theta = 21.78^\circ$ for the FM interlayer interaction amplitude $J_\perp/J = 0$. (c) Magnon band structures for the FM interlayer interaction amplitude $J_\perp/J = 0.2$. The zoom-ins demonstrate the dispersion around the K point.

constant of monolayer and the interlayer spacing between layers are both set to 1.

Magnon corner states induced by the FM interlayer coupling.—To diagnose the higher-order topology of the TBHM system with the FM interlayer coupling, we first calculate the magnon energy spectrum of the TBHM with a rhombus boundary preserving the twofold rotational symmetry. By numerically diagonalizing the magnon Hamiltonian Eq. (3) in real space, we plot the magnon energy spectrum in Fig. 1. It is found that the magnon energy spectrum shows an energy gap, and even more interestingly, two in-gap states reside in the energy gap [shown in Fig. 1(b)]. As shown in Fig. 1(c), the two in-gap states are symmetrically localized at the top and bottom corners of the rhombus, respectively, which are two mirror symmetric corners. Note that, due to the finite size effect, the two magnon corner states are not degenerate, and a small gap due to the hybridization of two corner states exists. The twofold symmetric in-gap corner states are a hallmark feature of the SOTMI in the TBHM, which are associated with a mirror winding number as demonstrated later in this paper.

In the SM [104], we demonstrate that the two mirror symmetric magnon corner states still exist when including remote intralayer and interlayer FM exchange couplings. Moreover, we also show that six magnon corner states appear when considering a finite hexagon-shaped TBHM sample in the SM. These magnon corner states are six-fold rotation symmetric and localized at the six corners of the sample.

Magnon band structures and mirror winding number. To gain more insight into the origin of magnon corner states, we study the bulk band structure of the TBHM and its topology. At the commensurate angle $\theta = 21.78^\circ$, the original translational symmetry of AA-stacked bilayer honeycomb is broken, but the moiré translational symmetry can be defined to display the periodicity of superlattices. Thereby, under the Fourier transformation, we obtain a 28×28 magnon Hamiltonian in the k space, which reads $H = \sum_{\mathbf{k}} \Psi_{\mathbf{k}}^\dagger H_{\mathbf{k}} \Psi_{\mathbf{k}}$ with the basis $\Psi_{\mathbf{k}}^\dagger = (c_{\mathbf{k},1}^\dagger, \cdots, c_{\mathbf{k},28}^\dagger)$. The concrete expression of $H_{\mathbf{k}}$ and more details are given in Ref. [104].

The magnon band structures of the TBHM system along a high symmetry line of the moiré Brillouin zone [see Fig. 2(a)] obtained by numerically diagonalizing $H_{\mathbf{k}}$ are shown in Fig. 2. For comparison, we also depict the magnon band structure of the TBHMs system in the absence of interlayer interaction $J_\perp/J = 0$ in Fig. 2(b). It is found that the magnon band structure shows linearly dispersive bands around the moiré Brillouin Zone corner **K**, which is identical to the monolayer honeycomb magnet. Subsequently, we present the magnon band structures of the TBHM system with a finite FM interlayer exchange interaction in Fig. 2(c), where we set $J_\perp/J = 0.2$ echoing the magnon energy spectrum of the system with open boundary conditions shown in Fig. 1. We conclude that the finite FM interlayer coupling opens a sizable energy gap at the point **K**. The energy gap is topologically nontrivial since magnon corner states emerge within it when the open boundary condition is imposed.

To further illustrate the topological properties of the magnon band structures, we utilize the $\mathbb{Z}_2$ mirror winding number [90] as a topological invariant to characterize the higher-order magnon topology. The mirror winding number ν is defined in a mirror-invariant line Γ-M-Γ in the moiré Brillouin zone, where C_{2x} symmetry is preserved. Then we can decompose the Hamiltonian $H_{\mathbf{k}}(k_x, 0)$, which situates at this mirror-invariant line Γ-M-Γ, into two decoupled parts $H_\pm(k_x)$ by projecting $H_{\mathbf{k}}(k_x, 0)$ onto the subspace formed by the eigenvectors that correspond to the mirror eigenvalues ± 1 of the mirror operator C_{2x}. The mirror winding number ν is defined as $\nu = \nu_+ = \nu_- \pmod 2$, where $\nu_\pm$ is the winding number in the two subsectors.

The mirror winding number can be calculated by the Wilson loop method [60,90,106]. The Wilson loop operator $W_\pm$ is considered in the mirror-invariant line Γ-M-Γ, where $k_i(k_f)$ is the initial (final) point of the loop. We define the element of a matrix $F_{x,k_i}^\pm$ as $[F_{x,k_i}^\pm]^{mn} = \langle u_{\pm,k_i+\Delta k}^n | u_{\pm,k_i}^n \rangle$, where Δk is the spacing of momentum in the loop and $|u_{\pm,k_x}^n\rangle$, for $n = 1 \ldots N_{occ}$, are the occupied Bloch functions of a crystal with N_{occ} occupied energy bands. Next, the Wilson loop operator can be expressed as $W_\pm = F_{k_f-\Delta k}^\pm F_{k_f-2\Delta k}^\pm \cdots F_{k_i+\Delta k}^\pm F_{k_i}^\pm$. Therefore, the winding number reads

$$\nu_\pm = \frac{1}{i\pi} \log(\det[W_\pm]). \tag{4}$$

In this work, the magnon corner states appear when the mirror winding number is $\nu = \nu_\pm = +1$, which confirms the topological origin of the magnon corner states localized at the mirror invariant corners of the TBHM.

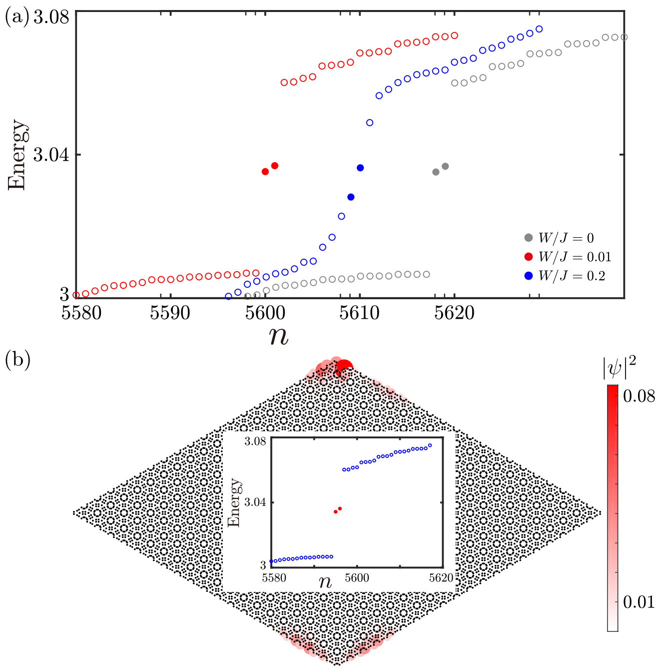

FIG. 3. (a) Magnon energy spectrum of the total Hamiltonian $H + H_z$ versus the eigenvalue index n. Red dots mark all the in-gap states. For comparison, we also plot the magnon energy spectrum (shown in grey circles and dots) without disorder ($W/J = 0$) and the magnon energy spectrum (shown in blue circles and dots) with strong disorder ($W/J = 0.2$). We take the model parameters $J_\perp/J = 0.2$, $W/J = 0.01$ and lattice site number $N = 11200$. (b) Magnon energy spectrum of the Hamiltonian H on the TBHMs system with a defect versus the eigenvalue index n, and the probability density of the two in-gap states, where $J_\perp/J = 0.2$ and the lattice site number $N = 11190$. Red dots mark all the in-gap states. The color map shows the values of the probability density.

Stability of corner states. Here, we use a random magnetic field to examine the robustness of the magnon corner states. The Zeeman term induced by the random magnetic field along z direction can be expressed as

$$H_z = -\sum_{i,l} B_{i,l}\mathbf{S}_{i,l}\cdot\mathbf{z}. \tag{5}$$

The random magnetic field is $B_i = W\omega_i$, where ω_i is the uniform random variable chosen from $[-0.5, 0.5]$ and W is the disorder strength. Within the framework of the linear spin-wave theory and via Holstein-Primakoff transformation, the Zeeman field term can be transformed into $H_z = \sum_{i,l} B_{i,l} d^\dagger_{i,l} d_{i,l}$, where all elements situate at the diagonal of the magnon Hamiltonian matrix, resembling the on-site chemical potential disorder known from the electronic version.

In Fig. 3(a), we demonstrate the magnon energy spectrum versus the eigenvalue index n for different disorder strength. We find that the two in-gap magnon corner states remain stable in the case of weak disorder, where we take the disorder strength as $W = 0.01$. While the in-gap magnon corner states are destroyed and pushed into bulk states by the strong disorder with the disorder strength ($W = 0.2$) shown in Fig. 3(a). In addition, we also reveal the robustness of the magnon corner states by introducing a local defect into the rhombus boundary sample at the top corner, where the defect is constructed by removing 10 sites. In the presence of defects, we plot the magnon energy spectrum and the spatial probability density of the two in-gap states in Fig. 3(b). We can see that the two in-gap states are still stable and localized around the original two corners, although the spatial distribution becomes mirror asymmetric. Meanwhile, in the SM [104], we also show that the sixfold rotation symmetric magnon corner states are robust against random magnetic fields and local defects.

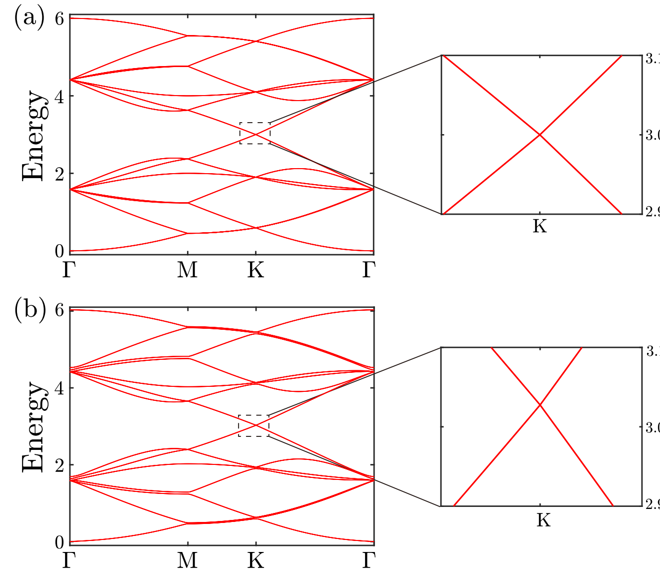

FIG. 4. (a) Magnon band structures of TBHMs with $\theta = 21.78^\circ$ for the AFM interlayer interaction amplitude $J_\perp/J = 0$, and (b) Magnon band structures for the AFM interlayer interaction amplitude $J_\perp/J = -0.2$. The zoom of the region near K point indicated by a dashed black box in the left panel of (a) and (b) are shown in the right panel.

AFM interlayer exchange coupling. We briefly discuss the case of AFM interlayer Heisenberg interaction in this section. We assume that the spins of the first (second) layer are polarized along the positive (negative) z direction. Similarly, using the Holstein-Primakoff transformation and neglecting magnon-magnon interactions, an effective magnon Hamiltonian H_{AFM} is obtained. Again by using the Fourier transformation, we obtain a 28×28 magnon Hamiltonian in the k space, which can be expressed as $H_{\mathrm{AFM}} = \sum_{\mathbf{k}} \psi^\dagger_{\mathbf{k}} H_{\mathrm{AFM}}(\mathbf{k})\psi_{\mathbf{k}}$ with the basis $\psi_{\mathbf{k}} = (c_{\mathbf{k},1}, \ldots, c_{\mathbf{k},14}, c^\dagger_{-\mathbf{k},15}, \ldots, c^\dagger_{-\mathbf{k},28})^T$. To obtain the AFM magnon band structures, we use a paraunitary Bogoliubov transformation $\psi_{\mathbf{k}} = R(\mathbf{k})\phi_{\mathbf{k}}$ to diagonalize the k-space magnon Hamiltonian as $R(\mathbf{k})^\dagger H_{\mathrm{AFM}}(\mathbf{k})R(\mathbf{k}) = D$, where D is a diagonal matrix and $\phi_{\mathbf{k}} = (1, \ldots, 1, -1, \ldots, -1)^T$. More details of the Hamiltonian in the AFM case are given in Ref. [104].

We display the AFM magnon band structures of the TBHM system in Fig. 4. Figure 4(a) shows the magnon band structure of the TBHMs system in the absence of the interlayer interaction, where we take the parameter $J_\perp/J = 0$. The magnon band structures of the TBHM system with a finite AFM interlayer interaction is shown in Fig. 4(b), where we set $J_\perp/J = -0.2$. It is found that, in contrast to the FM case, the AFM magnon energy bands of the system keep gapless, and the linear dispersion is stable, regardless of whether AFM interlayer interactions exist.

At last, it is necessary to point out that the ferromagnetic interlayer coupling induces the intervalley scattering of Dirac magnons, thus opens the energy gap, which is similar to the fermionic systems [90,107]. On the contrary, the antiferromagnetic coupling only involves the Dirac magnons within the same valley, which leaves them gapless.

Conclusion and Discussion. In this work, we have investigated higher-order topology of in the TBHM with the large commensurate angle $\theta = 21.78^{\circ}$. Based on a simple, minimal spin model, we found the FM interlayer coupling hybrids the Dirac bands of two individual honeycomb layers and thus opens a topological band gap characterized by the mirror winding number, leading to a SOTMI in the TBHM. The SOTMI supports hallmark magnon corner states, which are robust against weak random magnetic fields and local defects. In contrast, in the case of AFM interlayer coupling, the linearly dispersive magnon bands remain gapless.

Our theory is immediately testable considering rapid experimental progress on 2D twisted magnets [98–100]. Monolayer Chromium triiodide (CrI_3) is a 2D ferromagnet with honeycomb lattice [108]. For a $\theta = 21.78^{\circ}$ twisted bilayer CrI_3, our first-principles calculations show that interlayer FM interation is always favored, although its magnitude depends on the interlayer stacking configurations (See the calculations in the SM [104], also references [109–116] therein). Accordingly, we predict that twisted bilayer CrI_3 is a promising setup to realize the SOTMI featuring magnon corner states.

Acknowledgments. D.-H.X. was supported by the NSFC (under Grant Nos. 12074108 and 12147102) and the Natural Science Foundation of Chongqing (Grant No. CSTB2022NSCQ-MSX0568). B.Z. was supported by the NSFC (under Grant No. 12074107), the program of outstanding young and middle-aged scientific and technological innovation team of colleges and universities in Hubei Province (under Grant No. T2020001) and the innovation group project of the natural science foundation of Hubei Province of China (under Grant No. 2022CFA012). C.-Z.C. was funded by the National Key R&D Program of China (Grant No. 2022YFA1403700) and the NSFC (under Grant No. 11974256). C.-B.H was supported by the Doctoral Research Start-Up Fund of Hubei University of Science and Technology (under Grant No. BK202316).

[1] M. Z. Hasan and C. L. Kane, Colloquium: Topological insulators, Rev. Mod. Phys. **82**, 3045 (2010).
[2] X.-L. Qi and S.-C. Zhang, Topological insulators and superconductors, Rev. Mod. Phys. **83**, 1057 (2011).
[3] A. Bansil, H. Lin, and T. Das, Colloquium: Topological band theory, Rev. Mod. Phys. **88**, 021004 (2016).
[4] F. D. M. Haldane, Nobel Lecture: Topological quantum matter, Rev. Mod. Phys. **89**, 040502 (2017).
[5] X.-G. Wen, Colloquium: Zoo of quantum-topological phases of matter, Rev. Mod. Phys. **89**, 041004 (2017).
[6] P. Wölfle, Quasiparticles in condensed matter systems, Rep. Prog. Phys. **81**, 032501 (2018).
[7] H. Kondo, Y. Akagi, and H. Katsura, Non-Hermiticity and topological invariants of magnon Bogoliubov-de Gennes systems, Prog. Theor. Exp. Phys. **2020**, 12A104 (2020).
[8] Z.-X. Li, Y. Cao, and P. Yan, Topological insulators and semimetals in classical magnetic systems, Phys. Rep. **915**, 1 (2021).
[9] X. S. Wang and X. R. Wang, Topological magnonics, J. Appl. Phys. **129**, 151101 (2021).
[10] P. A. McClarty, Topological magnons: A review, Annu. Rev. Condens. Matter Phys. **13**, 171 (2022).
[11] Y. Onose, T. Ideue, H. Katsura, Y. Shiomi, N. Nagaosa, and Y. Tokura, Observation of the magnon Hall effect, Science **329**, 297 (2010).
[12] H. Katsura, N. Nagaosa, and P. A. Lee, Theory of the Thermal Hall Effect in Quantum Magnets, Phys. Rev. Lett. **104**, 066403 (2010).
[13] L. Zhang, J. Ren, J.-S. Wang, and B. Li, Topological magnon insulator in insulating ferromagnet, Phys. Rev. B **87**, 144101 (2013).
[14] A. Mook, J. Henk, and I. Mertig, Magnon Hall effect and topology in kagome lattices: A theoretical investigation, Phys. Rev. B **89**, 134409 (2014).
[15] A. Mook, J. Henk, and I. Mertig, Edge states in topological magnon insulators, Phys. Rev. B **90**, 024412 (2014).
[16] M. Hirschberger, R. Chisnell, Y. S. Lee, and N. P. Ong, Thermal Hall Effect of Spin Excitations in a Kagome Magnet, Phys. Rev. Lett. **115**, 106603 (2015).
[17] A. L. Chernyshev and P. A. Maksimov, Damped Topological Magnons in the Kagome-Lattice Ferromagnets, Phys. Rev. Lett. **117**, 187203 (2016).
[18] A. Mook, J. Henk, and I. Mertig, Spin dynamics simulations of topological magnon insulators: From transverse current correlation functions to the family of magnon Hall effects, Phys. Rev. B **94**, 174444 (2016).
[19] R. Seshadri and D. Sen, Topological magnons in a kagome-lattice spin system with XXZ and Dzyaloshinskii-Moriya interactions, Phys. Rev. B **97**, 134411 (2018).
[20] Y. Xing, H. Chen, N. Xu, X. Li, and L. Zhang, Valley modulation and single-edge transport of magnons in staggered kagome ferromagnets, Phys. Rev. B **105**, 104409 (2022).
[21] R. Chisnell, J. S. Helton, D. E. Freedman, D. K. Singh, R. I. Bewley, D. G. Nocera, and Y. S. Lee, Topological Magnon Bands in a Kagome Lattice Ferromagnet, Phys. Rev. Lett. **115**, 147201 (2015).
[22] H. Zhang, X. Feng, T. Heitmann, A. I. Kolesnikov, M. B. Stone, Y.-M. Lu, and X. Ke, Topological magnon bands in a room-temperature kagome magnet, Phys. Rev. B **101**, 100405(R) (2020).
[23] S. A. Owerre, Topological thermal Hall effect in frustrated kagome antiferromagnets, Phys. Rev. B **95**, 014422 (2017).
[24] S. K. Kim, H. Ochoa, R. Zarzuela, and Y. Tserkovnyak, Realization of the Haldane-Kane-Mele Model in a System of Localized Spins, Phys. Rev. Lett. **117**, 227201 (2016).
[25] S. A. Owerre, Topological honeycomb magnon Hall effect: A calculation of thermal Hall conductivity of magnetic spin excitations, J. Appl. Phys. **120**, 043903 (2016).

[26] S. A. Owerre, A first theoretical realization of honeycomb topological magnon insulator, J. Phys.: Condens. Matter **28**, 386001 (2016).
[27] S. A. Owerre, Floquet topological magnons, J. Phys. Commun. **1**, 021002 (2017).
[28] P. A. Pantaleón and Y. Xian, Effects of edge on-site potential in a honeycomb topological magnon insulator, J. Phys. Soc. Jpn. **87**, 064005 (2018).
[29] L.-C. Zhang, F. Zhu, D. Go, F. R. Lux, F. J. dos Santos, S. Lounis, Y. Su, S. Blügel, and Y. Mokrousov, Interplay of Dzyaloshinskii-Moriya and Kitaev interactions for magnonic properties of Heisenberg-Kitaev honeycomb ferromagnets, Phys. Rev. B **103**, 134414 (2021).
[30] A. Rückriegel, A. Brataas, and R. A. Duine, Bulk and edge spin transport in topological magnon insulators, Phys. Rev. B **97**, 081106(R) (2018).
[31] L. Chen, J.-H. Chung, B. Gao, T. Chen, M. B. Stone, A. I. Kolesnikov, Q. Huang, and P. Dai, Topological Spin Excitations in Honeycomb Ferromagnet CrI_3, Phys. Rev. X **8**, 041028 (2018).
[32] K. C. Xiaodong Cao and D. He, Magnon Hall effect on the Lieb lattice, J. Phys.: Condens. Matter **27**, 166003 (2015).
[33] S. Park and B.-J. Yang, Thermal Hall effect from a two-dimensional Schwinger boson gas with Rashba spin-orbit interaction: Application to ferromagnets with in-plane Dzyaloshinskii-Moriya interaction, Phys. Rev. B **102**, 214421 (2020).
[34] X. S. Wang, Y. Su, and X. R. Wang, Topologically protected unidirectional edge spin waves and beam splitter, Phys. Rev. B **95**, 014435 (2017).
[35] X. S. Wang, H. W. Zhang, and X. R. Wang, Topological Magnonics: A Paradigm for Spin-Wave Manipulation and Device Design, Phys. Rev. Appl. **9**, 024029 (2018).
[36] X. S. Wang, A. Brataas, and R. E. Troncoso, Bosonic Bott Index and Disorder-Induced Topological Transitions of Magnons, Phys. Rev. Lett. **125**, 217202 (2020).
[37] R. Shindou, J.-i. Ohe, R. Matsumoto, S. Murakami, and E. Saitoh, Chiral spin-wave edge modes in dipolar magnetic thin films, Phys. Rev. B **87**, 174402 (2013).
[38] R. Shindou, R. Matsumoto, S. Murakami, and J.-i. Ohe, Topological chiral magnonic edge mode in a magnonic crystal, Phys. Rev. B **87**, 174427 (2013).
[39] I. Lisenkov, V. Tyberkevych, A. Slavin, P. Bondarenko, B. A. Ivanov, E. Bankowski, T. Meitzler, and S. Nikitov, Spin-wave edge modes in finite arrays of dipolarly coupled magnetic nanopillars, Phys. Rev. B **90**, 104417 (2014).
[40] K. A. van Hoogdalem, Y. Tserkovnyak, and D. Loss, Magnetic texture-induced thermal Hall effects, Phys. Rev. B **87**, 024402 (2013).
[41] B. Li and A. A. Kovalev, Chiral topological insulator of magnons, Phys. Rev. B **97**, 174413 (2018).
[42] K. Nakata, S. K. Kim, J. Klinovaja, and D. Loss, Magnonic topological insulators in antiferromagnets, Phys. Rev. B **96**, 224414 (2017).
[43] K. H. Lee, S. B. Chung, K. Park, and J.-G. Park, Magnonic quantum spin Hall state in the zigzag and stripe phases of the antiferromagnetic honeycomb lattice, Phys. Rev. B **97**, 180401(R) (2018).
[44] A. Mook, B. Göbel, J. Henk, and I. Mertig, Taking an electron-magnon duality shortcut from electron to magnon transport, Phys. Rev. B **97**, 140401 (2018).
[45] H. Kondo, Y. Akagi, and H. Katsura, Three-dimensional topological magnon systems, Phys. Rev. B **100**, 144401 (2019).
[46] H. Kondo, Y. Akagi, and H. Katsura, $\mathbb{Z}_2$ topological invariant for magnon spin Hall systems, Phys. Rev. B **99**, 041110 (2019).
[47] J. Fransson, A. M. Black-Schaffer, and A. V. Balatsky, Magnon Dirac materials, Phys. Rev. B **94**, 075401 (2016).
[48] A. Mook, J. Henk, and I. Mertig, Tunable Magnon Weyl Points in Ferromagnetic Pyrochlores, Phys. Rev. Lett. **117**, 157204 (2016).
[49] Y. Su, X. S. Wang, and X. R. Wang, Magnonic Weyl semimetal and chiral anomaly in pyrochlore ferromagnets, Phys. Rev. B **95**, 224403 (2017).
[50] H. Kondo and Y. Akagi, Dirac Surface States in Magnonic Analogs of Topological Crystalline Insulators, Phys. Rev. Lett. **127**, 177201 (2021).
[51] Y.-H. Li and R. Cheng, Magnonic Su-Schrieffer-Heeger model in honeycomb ferromagnets, Phys. Rev. B **103**, 014407 (2021).
[52] S. A. Díaz, J. Klinovaja, and D. Loss, Topological Magnons and Edge States in Antiferromagnetic Skyrmion Crystals, Phys. Rev. Lett. **122**, 187203 (2019).
[53] F.-Y. Li, Y.-D. Li, Y. B. Kim, L. Balents, Y. Yu, and G. Chen, Weyl magnons in breathing pyrochlore antiferromagnets, Nat. Commun. **7**, 12691 (2016).
[54] K. Li, C. Li, J. Hu, Y. Li, and C. Fang, Dirac and Nodal Line Magnons in Three-Dimensional Antiferromagnets, Phys. Rev. Lett. **119**, 247202 (2017).
[55] A. Mook, J. Henk, and I. Mertig, Magnon nodal-line semimetals and drumhead surface states in anisotropic pyrochlore ferromagnets, Phys. Rev. B **95**, 014418 (2017).
[56] S. S. Pershoguba, S. Banerjee, J. C. Lashley, J. Park, H. Ågren, G. Aeppli, and A. V. Balatsky, Dirac Magnons in Honeycomb Ferromagnets, Phys. Rev. X **8**, 011010 (2018).
[57] W. Yao, C. Li, L. Wang, S. Xue, Y. Dan, K. Iida, K. Kamazawa, K. Li, C. Fang, and Y. Li, Topological spin excitations in a three-dimensional antiferromagnet, Nat. Phys. **14**, 1011 (2018).
[58] Y.-S. Lu, J.-L. Li, and C.-T. Wu, Topological Phase Transitions of Dirac Magnons in Honeycomb Ferromagnets, Phys. Rev. Lett. **127**, 217202 (2021).
[59] F. Zhu, L. Zhang, X. Wang, F. J. Dos Santos, J. Song, T. Mueller *et al.*, Topological magnon insulators in two-dimensional van der waals ferromagnets crsite3 and crgete3: Toward intrinsic gap-tunability, Sci. Adv. **7**, eabi7532 (2021).
[60] W. A. Benalcazar, B. A. Bernevig, and T. L. Hughes, Quantized electric multipole insulators, Science **357**, 61 (2017).
[61] F. Schindler, A. M. Cook, M. G. Vergniory, Z. Wang, S. S. Parkin, B. A. Bernevig, and T. Neupert, Higher-order topological insulators, Sci. Adv. **4**, eaat0346 (2018).
[62] J. Langbehn, Y. Peng, L. Trifunovic, F. von Oppen, and P. W. Brouwer, Reflection-Symmetric Second-Order Topological Insulators and Superconductors, Phys. Rev. Lett. **119**, 246401 (2017).
[63] Z. Song, Z. Fang, and C. Fang, $(d-2)$-Dimensional Edge States of Rotation Symmetry Protected Topological States, Phys. Rev. Lett. **119**, 246402 (2017).

[64] R. Chen, C.-Z. Chen, J.-H. Gao, B. Zhou, and D.-H. Xu, Higher-Order Topological Insulators in Quasicrystals, Phys. Rev. Lett. **124**, 036803 (2020).
[65] A. Sil and A. K. Ghosh, First and second order topological phases on ferromagnetic breathing kagome lattice, J. Phys.: Condens. Matter **32**, 205601 (2020).
[66] T. Hirosawa, S. A. Díaz, J. Klinovaja, and D. Loss, Magnonic Quadrupole Topological Insulator in Antiskyrmion Crystals, Phys. Rev. Lett. **125**, 207204 (2020).
[67] A. Mook, S. A. Díaz, J. Klinovaja, and D. Loss, Chiral hinge magnons in second-order topological magnon insulators, Phys. Rev. B **104**, 024406 (2021).
[68] Z. Li, Y. Cao, P. Yan, and X. Wang, Higher-order topological solitonic insulators, npj Comput. Mater. **5**, 107 (2019).
[69] Z.-X. Li, Y. Cao, X. R. Wang, and P. Yan, Second-order topological solitonic insulator in a breathing square lattice of magnetic vortices, Phys. Rev. B **101**, 184404 (2020).
[70] M. J. Park, S. B. Lee, and Y. B. Kim, Hinge magnons from noncollinear magnetic order in a honeycomb antiferromagnet, Phys. Rev. B **104**, L060401 (2021).
[71] I. Dzyaloshinsky, A thermodynamic theory of "weak" ferromagnetism of antiferromagnetics, J. Phys. Chem. Solids **4**, 241 (1958).
[72] T. Moriya, Anisotropic Superexchange Interaction and Weak Ferromagnetism, Phys. Rev. **120**, 91 (1960).
[73] Y. Cao, V. Fatemi, S. Fang, K. Watanabe, T. Taniguchi, E. Kaxiras, and P. Jarillo-Herrero, Unconventional superconductivity in magic-angle graphene superlattices, Nature **556**, 43 (2018).
[74] Y. Cao, V. Fatemi, A. Demir, S. Fang, S. L. Tomarken, J. Y. Luo *et al.*, Correlated insulator behaviour at half-filling in magic-angle graphene superlattices, Nature **556**, 80 (2018).
[75] R. Bistritzer and A. H. MacDonald, Moiré bands in twisted double-layer graphene, Proc. Natl. Acad. Sci. USA **108**, 12233 (2011).
[76] X. Lu, P. Stepanov, W. Yang, M. Xie, M. A. Aamir, I. Das *et al.*, Superconductors, orbital magnets and correlated states in magic-angle bilayer graphene, Nature **574**, 653 (2019).
[77] M. Yankowitz, S. Chen, H. Polshyn, Y. Zhang, K. Watanabe, T. Taniguchi, D. Graf, A. F. Young, and C. R. Dean, Tuning superconductivity in twisted bilayer graphene, Science **363**, 1059 (2019).
[78] A. L. Sharpe, E. J. Fox, A. W. Barnard, J. Finney, K. Watanabe, T. Taniguchi, M. A. Kastner, and D. Goldhaber-Gordon, Emergent ferromagnetism near three-quarters filling in twisted bilayer graphene, Science **365**, 605 (2019).
[79] G. Tarnopolsky, A. J. Kruchkov, and A. Vishwanath, Origin of Magic Angles in Twisted Bilayer Graphene, Phys. Rev. Lett. **122**, 106405 (2019).
[80] P. Stepanov, I. Das, X. Lu, A. Fahimniya, K. Watanabe, T. Taniguchi, F. H. L. Koppens, J. Lischner, L. Levitov, and D. K. Efetov, Untying the insulating and superconducting orders in magic-angle graphene, Nature **583**, 375 (2020).
[81] M. Serlin, C. L. Tschirhart, H. Polshyn, Y. Zhang, J. Zhu, K. Watanabe, T. Taniguchi, L. Balents, and A. F. Young, Intrinsic quantized anomalous Hall effect in a moiré heterostructure, Science **367**, 900 (2019).
[82] Y. Xie, B. Lian, B. Jack, X. Liu, C.-L. Chiu, K. Watanabe, T. Taniguchi, B. A. Bernevig, and A. Yazdani, Spectroscopic signatures of many-body correlations in magic-angle twisted bilayer graphene, Nature **572**, 101 (2019).
[83] Y. Jiang, X. Lai, K. Watanabe, T. Taniguchi, K. Haule, J. Mao, and E. Y. Andrei, Charge order and broken rotational symmetry in magic-angle twisted bilayer graphene, Nature **573**, 91 (2019).
[84] U. Zondiner, A. Rozen, D. Rodan-Legrain, Y. Cao, R. Queiroz, T. Taniguchi *et al.*, Cascade of phase transitions and Dirac revivals in magic-angle graphene, Nature **582**, 203 (2020).
[85] D. Wong, K. P. Nuckolls, M. Oh, B. Lian, Y. Xie, S. Jeon, K. Watanabe, T. Taniguchi, B. A. Bernevig, and A. Yazdani, Cascade of electronic transitions in magic-angle twisted bilayer graphene, Nature **582**, 198 (2020).
[86] H. C. Po, L. Zou, A. Vishwanath, and T. Senthil, Origin of Mott Insulating Behavior and Superconductivity in Twisted Bilayer Graphene, Phys. Rev. X **8**, 031089 (2018).
[87] H. C. Po, H. Watanabe, and A. Vishwanath, Fragile Topology and Wannier Obstructions, Phys. Rev. Lett. **121**, 126402 (2018).
[88] Z. Song, Z. Wang, W. Shi, G. Li, C. Fang, and B. A. Bernevig, All Magic Angles in Twisted Bilayer Graphene are Topological, Phys. Rev. Lett. **123**, 036401 (2019).
[89] J. Ahn, S. Park, and B.-J. Yang, Failure of Nielsen-Ninomiya Theorem and Fragile Topology in Two-Dimensional Systems with Space-Time Inversion Symmetry: Application to Twisted Bilayer Graphene at Magic Angle, Phys. Rev. X **9**, 021013 (2019).
[90] M. J. Park, Y. Kim, G. Y. Cho, and S. B. Lee, Higher-Order Topological Insulator in Twisted Bilayer Graphene, Phys. Rev. Lett. **123**, 216803 (2019).
[91] B. Liu, L. Xian, H. Mu, G. Zhao, Z. Liu, A. Rubio, and Z. F. Wang, Higher-Order Band Topology in Twisted Moiré Superlattice, Phys. Rev. Lett. **126**, 066401 (2021).
[92] M. J. Park, S. Jeon, S. Lee, H. C. Park, and Y. Kim, Higher-Order Topological Corner State Tunneling in Twisted Bilayer Graphene, Carbon **174**, 260 (2021).
[93] A. Chew, Y. Wang, B. A. Bernevig, and Z.-D. Song, Higher-order topological superconductivity in twisted bilayer graphene, arXiv:2108.05373.
[94] K. Hejazi, Z.-X. Luo, and L. Balents, Noncollinear phases in moiré magnets, Proc. Natl. Acad. Sci. USA **117**, 10721 (2020).
[95] D. Ghader, Magnon magic angles and tunable Hall conductivity in 2D twisted ferromagnetic bilayers, Sci. Rep. **10**, 15069 (2020).
[96] Y.-H. Li and R. Cheng, Moiré magnons in twisted bilayer magnets with collinear order, Phys. Rev. B **102**, 094404 (2020).
[97] X. Zhu, H. Guo, and S. Feng, Magnon bands in twisted bilayer honeycomb quantum magnets, Chin. Phys. B **30**, 077505 (2021).
[98] T. Song, Q.-C. Sun, E. Anderson, C. Wang, J. Qian, T. Taniguchi *et al.*, Direct visualization of magnetic domains and moiré magnetism in twisted 2D magnets, Science **374**, 1140 (2021).
[99] Y. Xu, A. Ray, Y.-T. Shao, S. Jiang, K. Lee, D. Weber *et al.*, Coexisting ferromagnetic–antiferromagnetic state in twisted bilayer CrI_3, Nat. Nanotechnol. **17**, 143 (2021).
[100] H. Xie, X. Luo, G. Ye, Z. Ye, H. Ge, S. H. Sung *et al.*, Twist engineering of the two-dimensional magnetism in double bilayer chromium triiodide homostructures, Nat. Phys. **18**, 30 (2022).

[101] M. Oudich, G. Su, Y. Deng, W. Benalcazar, R. Huang, N. J. R. K. Gerard, M. Lu, P. Zhan, and Y. Jing, Photonic analog of bilayer graphene, Phys. Rev. B **103**, 214311 (2021).

[102] C.-H. Yi, H. C. Park, and M. J. Park, Strongly coupled photonic moire superlattices, arXiv:2108.14002.

[103] S.-Q. Wu, Z.-K. Lin, B. Jiang, X. Zhou, B. Hou, and J.-H. Jiang, Observation of higher-order topological states in acoustic twisted moiré superlattice, arXiv:2105.14389.

[104] See Supplemental Material at http://link.aps.org/supplemental/10.1103/PhysRevB.107.L020404 for more details of the concrete expression of the k-spcae magnon Hamiltonian, the magnon corner states in the presence of long-range intralayer Heisenberg interactions, the details of the interlayer AFM Heisenberg interaction case, magnon corner states in a hexagon-shaped sample as well as the first principle calculations for the spin interactions in twisted bilayer CrI_3.

[105] T. Holstein and H. Primakoff, Field dependence of the intrinsic domain magnetization of a ferromagnet, Phys. Rev. **58**, 1098 (1940).

[106] W. A. Benalcazar, B. A. Bernevig, and T. L. Hughes, Electric multipole moments, topological multipole moment pumping, and chiral hinge states in crystalline insulators, Phys. Rev. B **96**, 245115 (2017).

[107] E. J. Mele, Commensuration and interlayer coherence in twisted bilayer graphene, Phys. Rev. B **81**, 161405 (2010).

[108] B. Huang, G. Clark, E. Navarro-Moratalla, D. R. Klein, R. Cheng, K. L. Seyler *et al.*, Layer-dependent ferromagnetism in a van der Waals crystal down to the monolayer limit, Nature **546**, 270 (2017).

[109] G. Kresse and J. Furthmüller, Efficient iterative schemes for *ab initio* total-energy calculations using a plane-wave basis set, Phys. Rev. B **54**, 11169 (1996).

[110] P. E. Blöchl, Projector augmented-wave method, Phys. Rev. B **50**, 17953 (1994).

[111] J. P. Perdew, K. Burke, and M. Ernzerhof, Generalized Gradient Approximation Made Simple, Phys. Rev. Lett. **77**, 3865 (1996).

[112] J. Klimeš, D. R. Bowler, and A. Michaelides, Van der Waals density functionals applied to solids, Phys. Rev. B **83**, 195131 (2011).

[113] A. I. Liechtenstein, V. I. Anisimov, and J. Zaanen, Density-functional theory and strong interactions: Orbital ordering in Mott-Hubbard insulators, Phys. Rev. B **52**, R5467 (1995).

[114] C. Xu, J. Feng, H. Xiang, and L. Bellaiche, Interplay between Kitaev interaction and single ion anisotropy in ferromagnetic CrI_3 and $CrGeTe_3$ monolayers, npj Comput. Mater. **4**, 57 (2018).

[115] C. Xu, J. Feng, S. Prokhorenko, Y. Nahas, H. Xiang, and L. Bellaiche, Topological spin texture in Janus monolayers of the chromium trihalides $Cr(I, X)_3$, Phys. Rev. B **101**, 060404(R) (2020).

[116] T. Olsen, Unified Treatment of Magnons and Excitons in Monolayer CrI_3 from Many-Body Perturbation Theory, Phys. Rev. Lett. **127**, 166402 (2021).